Magnetic Resonance Imaging of Spinal-Cord Hemangioblastoma

Murray Rebner[1] and Stephen S. Gebarski[2]

Myelography, computed tomography (CT), and angiography have been the imaging procedures of choice to evaluate hemangioblastomas [1–3]. There is a paucity of data available concerning the general imaging of spinal-cord-dominant lesions. Magnetic resonance (MR) imaging characteristics of a few cases of the more common posterior-fossa-dominant hemangioblastomas are available [4–6], but no case of MR of a spinal-cord-dominant lesion has been reported. For these reasons, we describe one patient with such a hemangioblastoma, both to illustrate an interesting case studied with conventional techniques and to compare these techniques with MR.

Case Report

A 34-year-old right-handed man experienced gradually increasing numbness in his hands over a 5 year period, at the end of which severe spasticity, incoordination, and hand weakness developed. Physical examination showed sensory loss over his shoulders and arms, grossly impaired position sense in his arms, spastic gait, and markedly increased tone in both hands. Cervical thoracic metrizamide myelography via a lumbar approach showed widening of the cervical and high thoracic spinal cord (fig. 1A). CT of the cervical spine, delayed 12 hr postmyelography, demonstrated diffuse spinal cord enlargement from C1 to T4 with subtle high attenuation seen within cord substance from C2 to C7 (fig. 1B). This high attenuation was not seen on 24 hr delayed CT, confirming it as pathologic spinal cord uptake of metrizamide.

Cranial CT showed an enhancing lesion consisting of high attenuation, serpiginous structures leading to a central high-attenuation nidus involving the posterior inferior cerebellar region. No low-attenuation region was seen about this lesion (figs. 1C and 1D). Arteriography demonstrated a hypervascular mass with prominent feeding

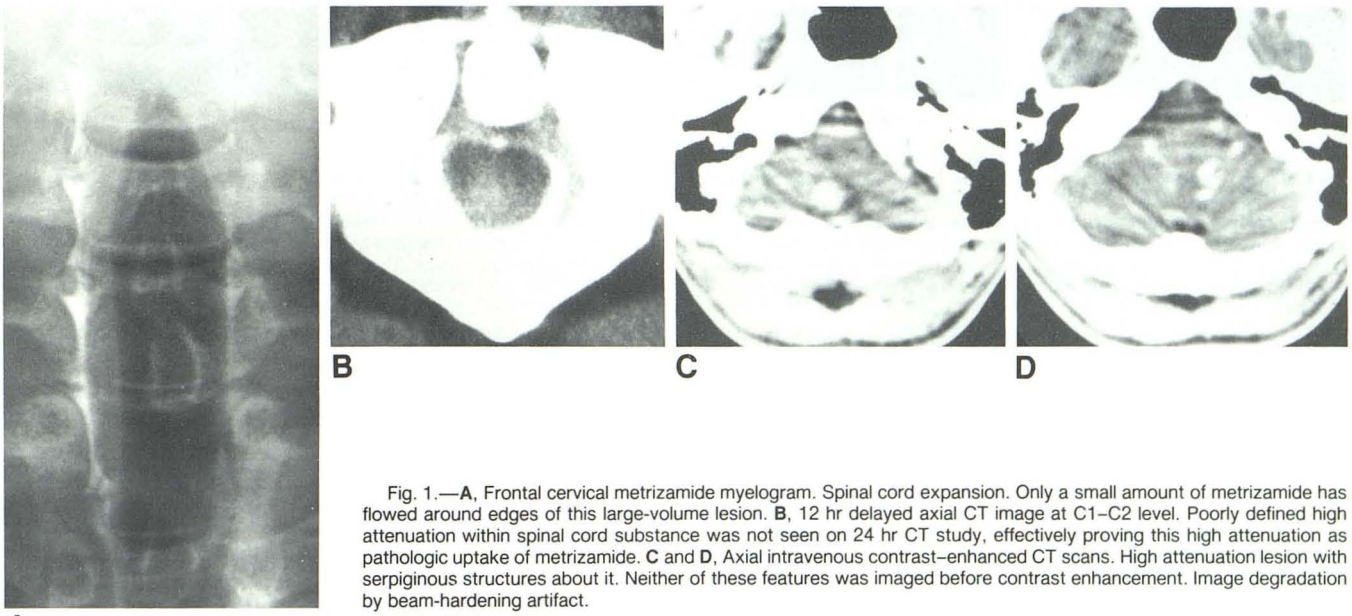

Fig. 1.—**A**, Frontal cervical metrizamide myelogram. Spinal cord expansion. Only a small amount of metrizamide has flowed around edges of this large-volume lesion. **B**, 12 hr delayed axial CT image at C1–C2 level. Poorly defined high attenuation within spinal cord substance was not seen on 24 hr CT study, effectively proving this high attenuation as pathologic uptake of metrizamide. **C** and **D**, Axial intravenous contrast–enhanced CT scans. High attenuation lesion with serpiginous structures about it. Neither of these features was imaged before contrast enhancement. Image degradation by beam-hardening artifact.

Received August 29, 1984; accepted after revision November 5, 1984.

[1] Department of Radiology, Division of Chest Radiology, University of Michigan Hospitals, Ann Arbor, MI 48109.

[2] Department of Radiology, Divisions of Neuroradiology and Magnetic Resonance Imaging, University of Michigan Hospitals, Ann Arbor, MI 48109. Address reprint requests to S. S. Gebarski.

AJNR **6:287–289, March/April 1985** 0195–6108/85/0602–0287 $00.00

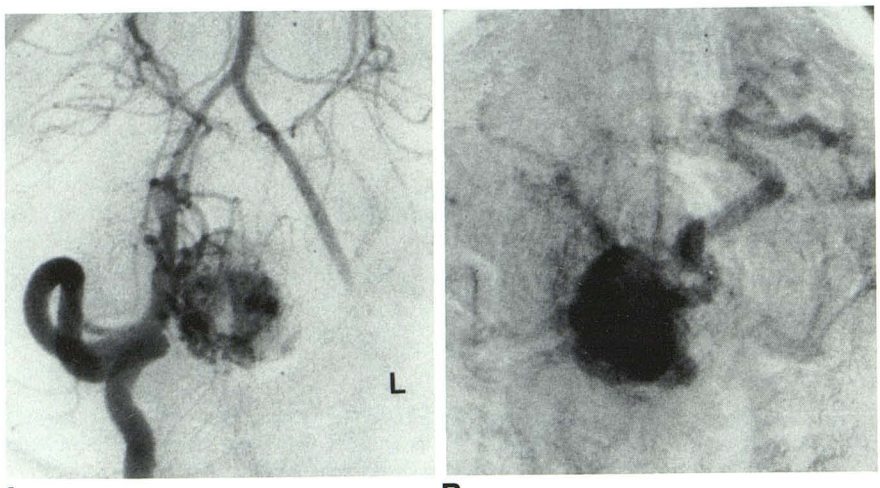

Fig. 2.—Submentovertex projections of right vertebral arteriogram. **A**, Early arterial phase. Hypervascular nidus; primary arterial supply is from tonsillohemispheric branches of right posterior inferior cerebellar artery. **B**, Late capillary/early venous stage. Persistent vascular "stain" in region of angiographically hypervascular nidus. Serpiginous pathologically dilated draining vein on left.

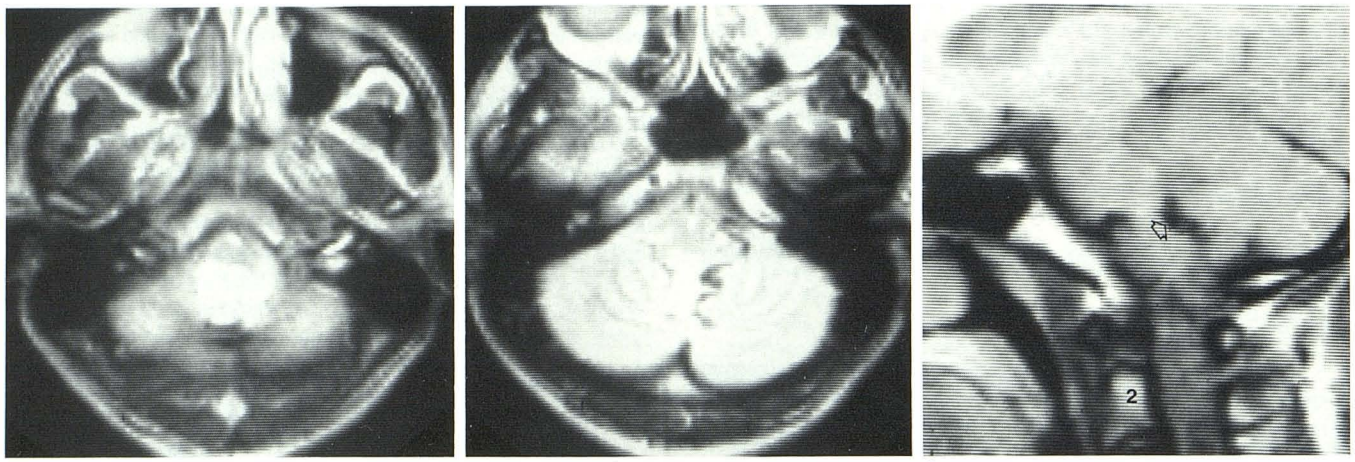

Fig. 3.—**A** and **B**, Axial SE 2000/56 images. High-signal nidus with serpiginous low-signal lesions immediately superior to nidus about medulla oblongata and right cerebellar tonsil. **C**, Sagittal SE 500/28 image. Intracranial part of image is slightly off midline, to the left, whereas high cervical spinal part of image is midline. Such an appearance results from slight head rotation. Extremely low-signal serpiginous lesion (*arrow*) immediately inferior to superior, displaced, somewhat distorted fourth ventricle and immediately superior to moderately low-signal-intensity nidus at foramen magnum. Well defined low-signal lesion occupies most of spinal cord substance from C2 to C3 level caudad. Dramatic change in signal characteristics of nidus in this T1-weighted vs. axial T2-weighted images. Persistent low-signal characteristics of serpiginous part of lesion and changing characteristics of nidus are totally consistent with arteriographic behavior. This single sagittal image demonstates all components of this complex lesion and shows their close topographic relation.

and draining vessels about the cervicomedullary junction and caudal cerebellum (fig. 2A). The "nidus" demonstrated persistent "stain" into the late venous phase (fig. 2B).

MR imaging was performed with a Diasonics 5 kG superconducting magnet operating at 3.5 kG, with spin-echo (SE) sequences imaging hydrogen nuclei. All scanning was performed with a head coil. Technical details were similar to those previously published [5]. No paramagnetic contrast material was used. Echo times (TEs) of 28 and 56 msec were obtained for all sequences discussed below. Imaging planes and repetition times (TRs) were as follows: (1) axial 2000 msec TRs, imaging 20 nearly contiguous 7 mm sections from the near vertex through the high cervical spinal cord; (2) coronal 1500 msec TRs, imaging 15 nearly contiguous 7 mm sections, including all of the posterior fossa and high cervical spinal cord up through the middle cranial fossa; and (3) sagittal 500 msec TRs, imaging five nearly contiguous 7 mm sagittal sections, including the upper cervical spinal cord, brainstem, and cerebellum.

Axial images were superior in delineating serpiginous, extremely low-signal aspects of the lesion extending to an extremely high-signal, well defined nidus about the posterior inferior cerebellar region (figs. 3A and 3B). The high-signal abnormality was seen to extend through to the high cervical spinal cord substance. Sagittal imaging again demonstrated the low posterior-fossa mass lesion, clearly delineating the superior displacement of the fourth ventricle and slight distortion of its floor (fig. 3C). This T1-weighted sagittal sequence showed the mass to have mixed low and moderate signal characteristics with direct contiguity through to the high spinal cord substance. Transition to a better defined, low-signal-intensity lesion occupying

nearly the entire spinal cord substance from C3 through the lowest segments scanned on the sagittal images, C7, was displayed on a single sagittal section.

The moderate- to low-signal-intensity characteristics of the nidus on these T1-weighted images and the marked increase in intensity on the T2-weighted axial and coronal images are consistent with a hypervascular hemangioma nodule. All sequences demonstrated the arterial supply and venous drainage as extremely low-intensity serpiginous structures, as would be expected by the rapid blood flow in these vessels [7]. The best etiology to explain all of these findings would be posterior fossa hemangioblastoma with spinal cord extension of its cystic component. Any other explanation for these MR findings would advance multiple different contiguous lesions such as posterior fossa mass with a second cystic mass lesion in the cervical spinal cord.

The patient underwent a posterior fossa craniectomy with gross removal of the nidus of a capillary hemangioblastoma about the foramen magnum. The spinal cord low-signal lesion proved to be the expected cystic extension of the hemangioblastoma into the cervical cord.

Discussion

Hemangioblastomas constitute about 7%–12% of primary adult posterior fossa tumors. The average age of onset of symptoms is the mid fourth decade, although patients with von Hippel-Lindau disease present earlier. The lesions tend to be slow-growing, and 10% of patients have more than one tumor. Most tumors are cystic, with small mural vascular nodules; however, 20–25% are solid. The lesion often is within the cerebellum and infrequently involves the medulla oblongata and spinal cord [1–3].

Typically, hemangioblastomas have a highly vascular component that causes a prominent "stain" during the capillary phase of angiography and persists into the late venous phase [3]. They can displace the fourth ventricle and may obstruct it [1]. Calcification is a rare finding. The lesion can present as either a dense nodule, a tangle of vessels, or both. Enlarged feeding arteries and draining veins may be seen with either type [3].

CT has been the imaging procedure of choice for posterior fossa masses. It is effective in demonstrating the relation of the lesion to the fourth ventricle, the cystic component of the lesion, and whether there is any obstructive hydrocephalus [1–3]. Angiography is more sensitive in detecting small hemangioblastomas and demonstrating the characteristic nodule usually related to a larger cystic component [3].

MR has been used for imaging intracranial and intraspinal lesions. Preliminary results comparing MR and CT have shown MR to be more sensitive than CT in the detection of central nervous sytem abnormalities, especially lesions of the posterior fossa and cervicomedullary junction [4–8]. MR also defines vascular structures resulting from inherent contrast differences between flowing blood and vessel wall. The signal intensity varies roughly inversely with blood flow, that is, high flow/low intensity [7]. Additional advantages of MR over other imaging methods include its biologic safety, after simple exclusions [9–11], and the availability of coronal and sagittal imaging planes without special patient positioning. Several limitations of MR include its inability to reliably detect calcification, poor specificity regarding many lesions, problems in differentiating surrounding edema from tumor, long image-acquisition time, and limited clinical availability [4–6, 8]. Although MR imaging does not obviate CT or angiography, it does provide complementary information in the diagnosis of hemangioblastoma. In our case of complex spinal-cord-dominant hemangioblastoma, MR was the only imaging technique that demonstrated all components of the lesion and their topographic relations.

ACKNOWLEDGMENT

We thank Sandra Ressler for assistance in manuscript preparation.

REFERENCES

1. Adair LB, Ropper AH, Davis KR. Cerebellar hemangioblastomas: computed tomographic, angiographic, and clinical correlation in 7 cases. *CT* **1978**;2:281–294
2. Ganti SR, Silver AJ, Hilal SK, Mawad ME, Sane P. Computed tomography of cerebellar hemangioblastomas. *CT* **1982**;6:912–919
3. Seeger JF, Burke DP, Knake JE, Gabrielsen TO. Computed tomographic and angiographic evaluation of hemangioblastomas. *Radiology* **1981**;138:65–73
4. Brant-Zawadzki M, Davis PL, Crooks LE, et al. NMR demonstration of cerebral abnormalities: comparsion with CT. *AJNR* **1983**;4:117–124, *AJR* **1983**;140:847–854
5. Brant-Zawadzki M, Badami JP, Mills CM, Norman D, Newton TH. Primary intracranial tumor imaging: a comparison of magnetic resonance and CT. *Radiology* **1984**;150:435–440
6. Randell CP, Collins AG, Young IR, et al. Nuclear magnetic resonance imaging of posterior fossa tumors. *AJNR* **1983**;4:1027–1034, *AJR* **1983**;141:489–496
7. Mills CM, Brant-Zawadzki M, Crooks LE, et al. Nuclear magnetic resonance: principles of blood flow imaging. *AJNR* **1983**;4:1161–1166 *AJR* **1984**;142:165–170
8. Hawkes RC, Holland GN, Moore WS, Kean DM, Worthington BS. NMR tissue characterization in intracranial tumors: preliminary results. *AJNR* **1983**;4:830–832
9. New PFJ, Rosen BR, Brady TJ, et al. Potential hazards and artifacts of ferromagnetic and nonferromagnetic surgical and dental materials and devices in nuclear magnetic resonance imaging. *Radiology* **1983**;147:139–148
10. Pavlicek W, Geisinger M, Castle L, et al. The effects of nuclear magnetic resonance on patients with cardiac pacemakers. *Radiology* **1983**;147:149–153
11. Schwartz JL, Crooks LE. NMR imaging produces no observable mutations or cytotoxicity in mammalian cells. *AJR* **1982**; 139:583–585